

Coupling Unbiased Mutagenesis to High-throughput DNA Sequencing Uncovers Functional Domains in the Ndc80 Kinetochores Protein of *Saccharomyces cerevisiae*

Jerry F. Tien,* Kimberly K. Fong,* Neil T. Umbreit,* Celia Payen,[†] Alex Zelter,* Charles L. Asbury,* Maitreya J. Dunham,[†] and Trisha N. Davis*¹

*Department of Biochemistry, [†]Department of Genome Sciences, and [‡]Department of Physiology and Biophysics, University of Washington, Seattle, Washington 98195

ABSTRACT During mitosis, kinetochores physically link chromosomes to the dynamic ends of spindle microtubules. This linkage depends on the Ndc80 complex, a conserved and essential microtubule-binding component of the kinetochore. As a member of the complex, the Ndc80 protein forms microtubule attachments through a calponin homology domain. Ndc80 is also required for recruiting other components to the kinetochore and responding to mitotic regulatory signals. While the calponin homology domain has been the focus of biochemical and structural characterization, the function of the remainder of Ndc80 is poorly understood. Here, we utilized a new approach that couples high-throughput sequencing to a saturating linker-scanning mutagenesis screen in *Saccharomyces cerevisiae*. We identified domains in previously uncharacterized regions of Ndc80 that are essential for its function *in vivo*. We show that a helical hairpin adjacent to the calponin homology domain influences microtubule binding by the complex. Furthermore, a mutation in this hairpin abolishes the ability of the Dam1 complex to strengthen microtubule attachments made by the Ndc80 complex. Finally, we defined a C-terminal segment of Ndc80 required for tetramerization of the Ndc80 complex *in vivo*. This unbiased mutagenesis approach can be generally applied to genes in *S. cerevisiae* to identify functional properties and domains.

ACCURATE chromosome segregation depends on the attachment between kinetochores and the dynamic ends of spindle microtubules. This attachment requires the Ndc80 complex, an essential and conserved microtubule-binding component of the kinetochore. *In vivo*, inactivation or depletion of Ndc80 complex components leads to detached kinetochores and severe chromosome segregation defects (reviewed in Kline-Smith *et al.* 2005). Mirroring kinetochore-microtubule linkages *in vivo*, recent experiments show that attachments between purified Ndc80 complexes and microtubule tips can persist throughout rounds of microtubule growth and shortening, can withstand tensile forces, can modulate microtubule dynamics, and can respond to regulation by mitotic

kinases (Guimaraes *et al.* 2008; Miller *et al.* 2008; Powers *et al.* 2009; Tien *et al.* 2010; DeLuca *et al.* 2011; Schmidt *et al.* 2012; Umbreit *et al.* 2012).

The Ndc80 complex (Figure 1) is a rod-shaped heterotetramer of Ndc80, Nuf2, Spc24, and Spc25 (Osborne *et al.* 1994; Janke *et al.* 2001; Wigge and Kilmartin 2001; Wei *et al.* 2005). The two ends of the complex have globular domains, formed by Ndc80/Nuf2 and Spc24/Spc25, respectively. All four components of the complex are predicted to participate in coiled-coil interactions that link these two globular ends. Structural studies of the complex at atomic resolution have been limited to the two globular domains, revealing a microtubule-binding calponin homology (CH) domain in Ndc80 (Wei *et al.* 2006, 2007; Ciferri *et al.* 2008).

These structural studies on the globular ends of the Ndc80 complex have provided high-resolution views of key protein-protein interfaces (Alushin *et al.* 2010; Malvezzi *et al.* 2013; Nishino *et al.* 2013). Together, they help explain how the Ndc80 complex plays a central role in kinetochore function by physically linking spindle microtubules

Copyright © 2013 by the Genetics Society of America
doi: 10.1534/genetics.113.152728

Manuscript received April 29, 2013; accepted for publication June 25, 2013

Supporting information is available online at <http://www.genetics.org/lookup/suppl/doi:10.1534/genetics.113.152728/-/DC1>.

¹Corresponding author: Box 357350, Department of Biochemistry, University of Washington, Seattle, WA 98195. E-mail: tdavis@uw.edu

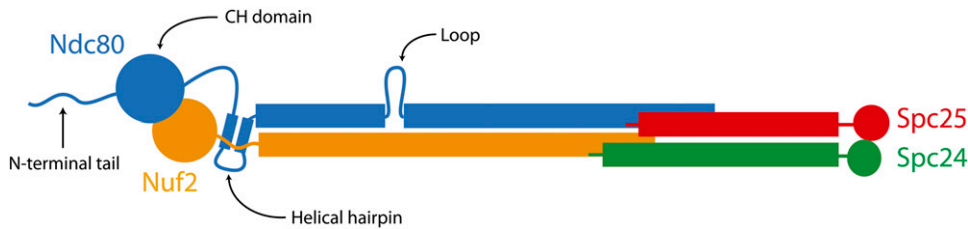


Figure 1 The Ndc80 complex contains Ndc80, Nuf2, Spc24, and Spc25.

to centromere-proximal kinetochore components. However, genetic and biochemical studies have suggested additional roles for the Ndc80 complex during mitosis. For example, mutations in *NDC80* result in mislocalization of kinetochore- and microtubule-associated proteins, such as the Dam1 complex and Stu2 in yeast (He *et al.* 2001; Janke *et al.* 2002). It is still unknown how the Ndc80 complex interacts with many of its proposed binding partners, and much of the complex is composed of long coiled-coil elements that have not been amenable to structural characterization. To identify the functionally important regions within Ndc80, we employed an unbiased linker-scanning mutagenesis screen. This screen utilizes short insertions at random positions within a protein to determine putative functional domains. Previous applications of linker-scanning mutagenesis have been successful in generating mutants to examine cohesin complex formation and Cre recombinase activity, and to map the Rab8A interaction interface on JFC1 (Petyuk *et al.* 2004; Milutinovich *et al.* 2007; Pajunen *et al.* 2007). Here, we comprehensively covered *NDC80* with 15-bp insertions at random positions, and the resulting mutant library was screened for viability in a red/white plasmid shuffle assay. High-throughput Illumina sequencing showed that lethal mutations fell into clusters, revealing several regions of Ndc80 that are essential for its function. These include the microtubule-binding domain, the helical hairpin, the tetramerization domain, and previously uncharacterized segments. Our approach, which couples unbiased mutagenesis to high-throughput sequencing, can be generally applied to reveal new functional domains of proteins in *Saccharomyces cerevisiae*.

Materials and Methods

Media

The compositions of YPD (yeast peptone dextrose rich) and SD (synthetic dextrose minimal) media were previously described (Burke *et al.* 2000). YPD-NAT medium is YPD with 25 $\mu\text{g}/\text{ml}$ nourseothricin (clonNAT, Werner BioAgents). SD-lys medium was described previously (Nguyen *et al.* 1998). SD-ura low ade is SD medium containing 100 $\mu\text{g}/\text{ml}$ tryptophan, 0.1% casamino acids, and 5 $\mu\text{g}/\text{ml}$ adenine.

Plasmids

All plasmids used in this study are listed in Supporting Information, Table S1. QuikChange Lightning site-directed mutagenesis (Stratagene) was used to construct plasmids containing lethal mutations in *NDC80*.

Strains

All yeast strains used in this study were derived from W303 and are listed in Table S2. To make the strain used in the linker-scanning mutagenesis screen, JTY5-5C, the endogenous copy of *NDC80* was deleted by PCR amplifying a *NatMX* cassette from pKG9 using primers with homology to the flanking DNA of *NDC80*. The deletion cassette was then transformed into the diploid strain JTY1 and selected for on YPD-NAT to generate JTY4. The deletion was checked by PCR to ensure replacement of *NDC80* with the cassette. JTY4 was transformed with the “*ADE3* plasmid” (pJT12) containing *ADE3 LYS2 NDC80* and selected for on SD-lys. The transformants were sporulated and dissected to obtain JTY5-5C.

Linker-scanning mutagenesis

A “target plasmid” (pJT36) was constructed containing the wild-type *NDC80* gene (including 245 upstream and 299 downstream base pairs), the ampicillin resistance gene, and the *URA3* gene for selection. Importantly, this plasmid did not contain a *NotI* recognition sequence. Using the MuA transposase, an artificial transposon was inserted at a random location within the target plasmid (Finnzymes). Transposition efficiency was kept low so that, on average, each plasmid would contain only one transposon insertion. The transposon contains a kanamycin resistance gene flanked by the 8-bp *NotI* recognition sequence. Plasmids that contained a transposon were isolated by selection on kanamycin. These plasmids were then cut with *NotI* to remove the kanamycin cassette and then religated. The resulting “transposition library” contained plasmids that each have 15 bp inserted at a random location. Each 15-bp insertion contained 5 bp of duplicated target sequence and the *NotI* recognition sequence.

Red/white plasmid shuffle screen

To identify lethal insertions in *NDC80*, the transposition library was screened in *S. cerevisiae* using a red/white plasmid shuffle system (Davis 1992; Muller 1996). This screen was carried out in the strain JTY5-5C (*ade2-1oc ade3 Δ -100 ura3-1 ndc80 Δ ::NatMX*), transformed with pJT12 (*NDC80 ADE3* in a 2- μm vector). In an *ade2-1oc ade3 Δ -100* background, yeast containing this *ADE3* plasmid produce a red pigment when grown on low adenine plates (Bender and Pringle 1991). The transposition library was transformed into this strain and selected for growth on SD-ura low ade plates at 37°. Insertions that abolish the function of *NDC80* are lethal and render cells dependent on the *ADE3* plasmid

with the wild-type copy of *NDC80* for survival. Therefore, lethal mutations can be identified as those that yield solid red colonies. Insertions that do not disrupt the function of *NDC80* have no effect on cell viability, making the *ADE3* plasmid extraneous. These colonies have a sectored appearance—red in the center and white around the edges where the *ADE3* plasmid was lost. Nonsectored red colonies, containing lethal mutations, were isolated and their plasmid DNA was extracted for sequencing.

We determined that the false-positive rate of the red/white plasmid shuffle screen is <0.3%. This was accomplished by transforming JTY5-5C [pJT12] with a plasmid containing wild-type *NDC80* (pJT36) and counting the number of nonsectored colonies. These false positives therefore represent colonies that were solid red despite the presence of a second wild-type copy of the gene. The representative lethal insertions selected for characterization (see below) were also retested in the red/white plasmid shuffle assay. JTY5-5C [pJT12] cells transformed with plasmids containing these insertions were confirmed to not sector.

Illumina sequencing

Illumina sequencing was used to determine the coverage of insertions in the transposition library and to identify the location of each lethal insertion obtained from the solid red colonies. Using the Expand Long Template PCR System (Roche), *NDC80* was amplified both from the transposition library and the pooled lethal mutants. In this PCR, primers were designed to specifically amplify the mutant alleles from the transposition library plasmids and not *NDC80* from the *ADE3* plasmid (Table S3). Single-end Illumina libraries were prepared from PCR products that were sheared to an average size of 500 bp by sonication. The sheared DNA ends were repaired using the End-It DNA repair kit (Epicentre), and A-tailed for ligation of adaptors (Table S3). The products were size selected (250–350 bp) and enriched by PCR using the primers presented in Table S3. Unique 6-bp indices on the PCR primers permitted multiplexed Illumina sequencing to distinguish between products from the transposition library and the pooled lethal mutants. One sequencing run of the transposition library and both sequencing runs of the lethal insertion subsets were alternatively prepared using the TruSeq DNA Sample Preparation v2 Kit. Briefly, PCR products were sheared to an average size of 500 bp using a Covaris E210. The sheared DNA ends were repaired and adenylated using the TruSeq protocol. Adapters AD002, AD018, and AD019 (Table S3) were ligated onto the transposition library sample and the two lethal insertion subset samples, respectively. The products were size selected (400–500 bp) and enriched by PCR using the TruSeq PCR Master Mix. All sequencing was performed on an Illumina Genome Analyzer II, to obtain 36-bp single reads. Sequencing results are provided in Table S4.

Custom programs (available upon request) were used to analyze the FASTQ files for each Illumina sequencing run. The 36-bp reads were queried for the *NotI* recognition

sequence; for each hit, the position of the *NotI* sequence within the read was recorded. The sequences flanking each *NotI* insertion were then aligned to the *NDC80* gene using mrsFAST (Hach *et al.* 2010) to determine the position of the insertion in *NDC80*. Read coverage was obtained by aligning all reads (with and without *NotI*) to *NDC80* using mrsFAST. Each 15-bp insertion was also translated to determine the protein sequence of the five inserted amino acids. See Table 1 for examples of insertion positions, resulting sequences, and the translated insertion residues.

We selected representative mutations from each lethal insertion cluster for further analysis. Each mutation represents the insertion with one of the highest number of *NotI* reads in the cluster. For further characterization, we required that each insertion was lethal at both the screening temperature of 37° and additionally 24°. Based on these criteria, we selected ins506, ins656, ins839, ins940, ins1148, ins1687, and ins1957 (Table 1) for further analysis.

Coiled-coil prediction and sequence alignment of Ndc80

The probabilities of coiled-coil formation for wild-type and mutant *Ndc80* were predicted using Paircoil2 (McDonnell *et al.* 2006). To perform sequence alignments, *NDC80* from *S. cerevisiae* and its orthologs in *Saccharomyces bayanus*, *S. kudriavzevii*, *S. mikatae* (Scannell *et al.* 2011), *Lachancea (Kluyveromyces) thermotolerans*, *Kluyveromyces lactis*, and *Debaryomyces hansenii* (<http://genolevures.org>) were translated using Transeq (Rice *et al.* 2000) and then aligned using Clustal-O (Blackshields *et al.* 2010). The similarity score was plotted for each position using Plotcon (Rice *et al.* 2000) with a window size of 21 bp.

Protein expression and purification

Recombinant *S. cerevisiae* *Ndc80* and *Dam1* complexes were expressed and purified as previously described (Miranda *et al.* 2005; Wei *et al.* 2005; Asbury *et al.* 2006; Powers *et al.* 2009).

Immunoprecipitation

JTY29-1C (*NUF2-TAP*) and JTY47-2B (*SPC24-TAP*) were transformed with plasmids encoding wild-type or mutant *GFP-NDC80* (Table S1) and selected for growth on SD-ura at 24°. Controls for the immunoprecipitation include JTY29-1C and JTY47-2B transformed with pRS316, as well as JTY29-1B (*NUF2*) and JTY47-2A (*SPC24*) transformed with a wild-type *GFP-NDC80* plasmid. Cells were grown to ~100 Klett units in 50 ml SD-ura at 24° and washed with dH₂O, and the pellets were frozen in liquid nitrogen. Pellets were resuspended in 500 µl lysis buffer (20 mM HEPES, pH 7.4, 300 mM NaCl, 100 µM GTP, 1 mM MgCl₂, 1 mM dithiothreitol, 4 µg/ml pepstatin, 4 µg/ml leupeptin, 4 µg/ml aprotinin, 4 µg/ml chymostatin, 1 mM phenylmethanesulfonyl fluoride, 1 mM sodium pyrophosphate, 1 mM sodium fluoride, 1 mM β-glycerophosphate, 5% glycerol) and vortexed with ice-cold glass beads in 1-min intervals until >60% of cells were lysed. Triton X-100 was added to 0.5% and lysates were cleared by centrifugation at 18,000 × *g*

Table 1 Representative lethal insertions in *NDC80*

Insertion position	Sequence ^a	Inserted residues	First mutation	<i>In vivo</i> expression ^b	Kinetochore localization ^c
506	TTCAAGTGGTT TCGGCCG CAGTGGTTATAT	LRPQW	Y170R	+	–
656	CACAAATTTCT TCGGCCG CAATTTCTTGGC	LRPQF	G220R	+	+
839	AAACTGTTAAT TCGGCCG CAGTTAATTGAT	MRPQL	I280M	+	+
940	ATTCGTTCACT TCGGCCG CATTACATAAT	CGRIH	I314C	+	+
1148	AAGATGAAAT TCGGCCG CAGAAATCCGAG	LRPQK	S383L	+	+
1687	GAAAACCAAT TCGGCCG CACTCAAATTA	CGRTQ	I563C	+	+
1957	TATTGATATAT TCGGCCG CAATATAACAAG	CGRNI	T653C	+	–

^a 15-bp insertions are in boldface text.

^b Figure 3E.

^c Figure 5, A and B.

for 20 min at 4°. An aliquot (50 μ l) of 60 mg/ml Dynabeads (Invitrogen) conjugated with rabbit IgG (MP Biomedicals) was added to the clarified lysate and incubated for 30 min at 4°. Beads were then washed with 150 μ l of wash buffer (20 mM HEPES, pH 7.4, 200 mM NaCl, 100 μ M GTP, 1 mM MgCl₂, 5% glycerol) three times and resuspended in 50 μ l of SDS–PAGE sample buffer.

Fluorescence microscopy

For live-cell imaging, JTY12-25A (*NUF2-mCherry NDC80*) was transformed with plasmids encoding wild-type or mutant *GFP–NDC80* (Table S1) and selected for growth on SD–ura at 24°. Cells were mounted for microscopy as previously described (Muller *et al.* 2005). Images of cells were taken at a single focal plane, binned 1 \times 1, using a DeltaVision system (Applied Precision) equipped with an IX70 inverted microscope (Olympus), an U Plan Apo 100 \times objective (1.35 NA), and a CoolSnap HQ digital camera (Photometrics). Exposures were 0.4 sec for both GFP and mCherry. Images were processed as previously described (Shimogawa *et al.* 2010) using custom Matlab programs (available upon request) to isolate and quantify the fluorescence intensities of GFP and mCherry spots.

Total internal reflection fluorescence (TIRF) microscopy was performed as previously described (Tien *et al.* 2010), with the following modifications. A custom TIRF illumination system was constructed by modification of a commercial inverted microscope (Nikon Ti-U). Total internal reflection of 488 nm (Sapphire 488-100 CW, Coherent Inc.) and 561 nm (Sapphire 561-100 CW, Coherent Inc.) wavelength lasers was achieved using a through-the-objective arrangement with a 100 \times oil immersion 1.49 NA lens (Nikon CFI APO 100 \times Oil TIRF NA 1.49 WD 0.12 mm). Simultaneous imaging of GFP and Alexa Fluor 568 was captured by two cooled EM CCD cameras (iXon+ DU897, Andor Technology). Flow cell channels were constructed using double-sided sticky tape (Scotch), sandwiched between a glass slide (Gold Seal) and silanized coverslip (Corning). To bind taxol-stabilized microtubules, a modified “rigor” kinesin was flowed into the channel and bound nonspecifically to the coverslip. The flow cell channel was washed with 50 μ l BB80 (80 mM Pipes, 120 mM K⁺, 1 mM MgCl₂, 1 mM EGTA,

8 mg/ml BSA, pH 6.9) and 50 μ l BB80T (BB80 with 10 μ M taxol). Alexa Fluor 568-labeled microtubules diluted in BB80T were flowed in and allowed to bind for 5 min. The channel was washed once more with 50 μ l BB80T. Proteins were then introduced, diluted in BB80T containing 0.1 mg/ml κ -casein, 200 μ g/ml glucose oxidase, 35 μ g/ml catalase, 25 mM glucose, and 5 mM dithiothreitol. GFP-tagged *Ndc80* complex was assayed at 50 pM to resolve single molecules, and untagged *Dam1* complex was added at 2.5 nM. Flow cell channels were sealed with nail polish and immediately imaged for 1500 frames at 10 frames per second. Software analysis of TIRF microscopy data was performed using custom software (available upon request) in Labview (National Instruments) and Igor Pro (WaveMetrics), as previously described (Tien *et al.* 2010).

Results

Construction of the linker-scanning transposition library

To discover new functional domains in the *Ndc80* kinetochore protein (Figure 1), we performed a saturating screen that combined linker-scanning mutagenesis with a plasmid shuffle colorimetric assay and high-throughput sequencing. We first constructed a transposition library using an artificial transposition system (Figure 2A; *Materials and Methods*). This library contains a collection of plasmids, each with a single 15-bp insertion at a random location, corresponding to a five-amino-acid insertion in the translated protein product. Our *NDC80* transposition library was generated from \sim 11,000 transposition events on a 7.4-kb plasmid, which includes the 2.1-kb *NDC80* gene. Each 15-bp insertion contained the 8-bp *NotI* recognition sequence, which was used to identify the position of the insertion within the gene.

Insertion coverage of the *NDC80* gene was determined by Illumina sequencing (Figure 3, A–D, and Figure S1). From three independent sequencing runs, we determined that transpositions targeted 1074 unique positions on *NDC80*, corresponding to 52% coverage of the 2076-bp gene (see Table S4 for a summary of the sequencing study). Furthermore, insertions were spread evenly across *NDC80*, with an average of 10.8 insertions per 21-bp window across the entire gene

(Figure 3D, right plot). From the 1074 insertion positions identified in the library, the translated protein sequences were determined. The frame of each insertion and its surrounding wild-type *NDC80* sequence ultimately dictates the identity of the amino acids inserted into the protein (Figure S2A). By experimental design, the insertions did not introduce stop codons and were always 15 bp long to prevent frame shifts in the resulting coding sequence (Figure S2A). The transposon library contained insertions at 444 unique codons, resulting in 64% coverage of the 691-amino-acid Ndc80 protein. Of these insertions, 30% were in frame 1, 26% were in frame 2, and 44% were in frame 3 (Figure S2B). The transposon library was then screened in *S. cerevisiae* to identify mutations that disrupt the function of Ndc80.

Linker-scanning mutagenesis screen of Ndc80

A red/white plasmid shuffle system (Davis 1992; Muller 1996) was used to screen the transposon library for insertions detrimental to the function of *NDC80* in *S. cerevisiae* (Figure 2B). In this screen, colonies containing library plasmids with lethal mutations in *NDC80* do not sector and are solid red (see *Materials and Methods*). We screened 25,439 total colonies and isolated 959 red colonies (4%). These red colonies were pooled and the positions of the insertions were determined by Illumina sequencing (Table S4). Lethal insertions were found at 336 unique positions in 162 unique codons of *NDC80*, corresponding to 16% coverage of the gene and 23% of the protein. Unlike the transposon library, in which insertions were found evenly spread throughout the *NDC80* gene, plasmids isolated from the red colonies contained insertions that mapped to distinct clusters (Figure S1). This was most evident on a coverage density map, showing the number of lethal insertions in 21-bp windows across *NDC80* (Figure 3D). We defined a stretch of lethal insertions as a cluster if four or more insertions per 21-bp window were lethal (Figure 3D). In several windows within these clusters, every single insertion present in the transposon library was lethal. Surprisingly, lethal insertions were not enriched in any particular frame relative to the transposon library (Figure S2B). Furthermore, each of the three frames was well represented in all of the clusters identified (Figure S2C). These results suggest that the position of the insertion, rather than the identity of the residues, was most important in disrupting the function of Ndc80.

To verify that the clusters identified in our screen are not a result of random sampling, we divided the nonsectoring red colonies into two random pools. When sequenced independently (Table S4), both subsets had the same lethal insertion clusters as the original pool (Figure S3), indicating we have comprehensively screened the starting transposon library. Overall, our screen demonstrates that five-amino-acid insertions are tolerated throughout most of Ndc80 without disrupting its function. We did not identify lethal insertions in the putative “loop” (Figure 3A, blue bar), nor in a segment of Ndc80 that is disordered based on the human Ndc80 globular domain crystal structure (Figure 3A, black bar)

(Ciferri *et al.* 2008). No lethal insertion clusters were found in the 113-amino acid N-terminal tail of Ndc80, which is dispensable in *S. cerevisiae* (Akiyoshi *et al.* 2009; Kemmler *et al.* 2009). Likewise, there were no lethal insertion clusters in the last ~30 amino acid residues of Ndc80, consistent with the viability of the *ndc80-1* temperature-sensitive allele, which contains a frameshift mutation that alters the last 18 amino acids of the protein (Wigge *et al.* 1998).

From the lethal insertion clusters identified in the linker-scanning mutagenesis screen, we selected representative mutations for further analysis. These lethal insertions are referred to as, for example, “ins506” to indicate that the first position of the insertion is nucleotide 506 of the mutant allele. A representative insertion from each cluster was independently verified to be lethal (see *Materials and Methods*). Insertions from the cluster around nucleotide 1400 of *NDC80* were found to be temperature sensitive; six insertions from this cluster, ranging from nucleotide 1380 to 1406, were lethal at 37° but not 24°. Therefore, this cluster was omitted from further analysis. Here, we selected a total of seven representative mutations from the remaining lethal insertion clusters for analysis (Table 1). We first tested if these mutations perturb protein expression or assembly of Ndc80 into a heterotetrameric complex. *In vivo*, all seven lethal insertion mutant alleles were expressed (Figure 3E). In these cells, the endogenous wild-type copy of *NDC80* was maintained for viability. A GFP tag on the mutant Ndc80 was used to distinguish it from the wild-type protein. In a recombinant expression system, six of the seven mutant Ndc80 proteins copurified as heterotetrameric complexes with Nuf2, Spc24, and Spc25 (Figure 3F). These results suggest that most of the insertions identified in this screen specifically disrupt the function of Ndc80 independent from protein production and folding.

Lethal insertions in the Ndc80 microtubule-binding domain

Two of the seven clusters of lethal insertions (represented by ins506 and ins656) are in the conserved microtubule-binding CH domain (Figure 3, A–D and Figure 4A). Based on homology to the human Ndc80 CH domain crystal structure (Ciferri *et al.* 2008), these lethal insertion clusters map to helices α C and α G, respectively. Even though these helices are adjacent in the crystal structure, the two mutations had drastically different effects. Ndc80 containing the ins506 mutation was expressed *in vivo* (Figure 3E), but failed to assemble into a recombinant complex. Consistent with our conclusion that the position of the insertion is likely most important in disrupting the function of Ndc80, we found that the ins511 mutation, which overlaps ins506 by 10 bp but is in a different frame, also impairs assembly of Ndc80 into a recombinant complex. By contrast, we successfully purified ins656 Ndc80 complex and further demonstrated that this complex binds microtubules *in vitro* (Figure 3F and Figure S4). Two additional clusters of lethal insertions (represented by ins839 and ins940) were found in a region of Ndc80 that folds into a helical hairpin (α H and α I) in the

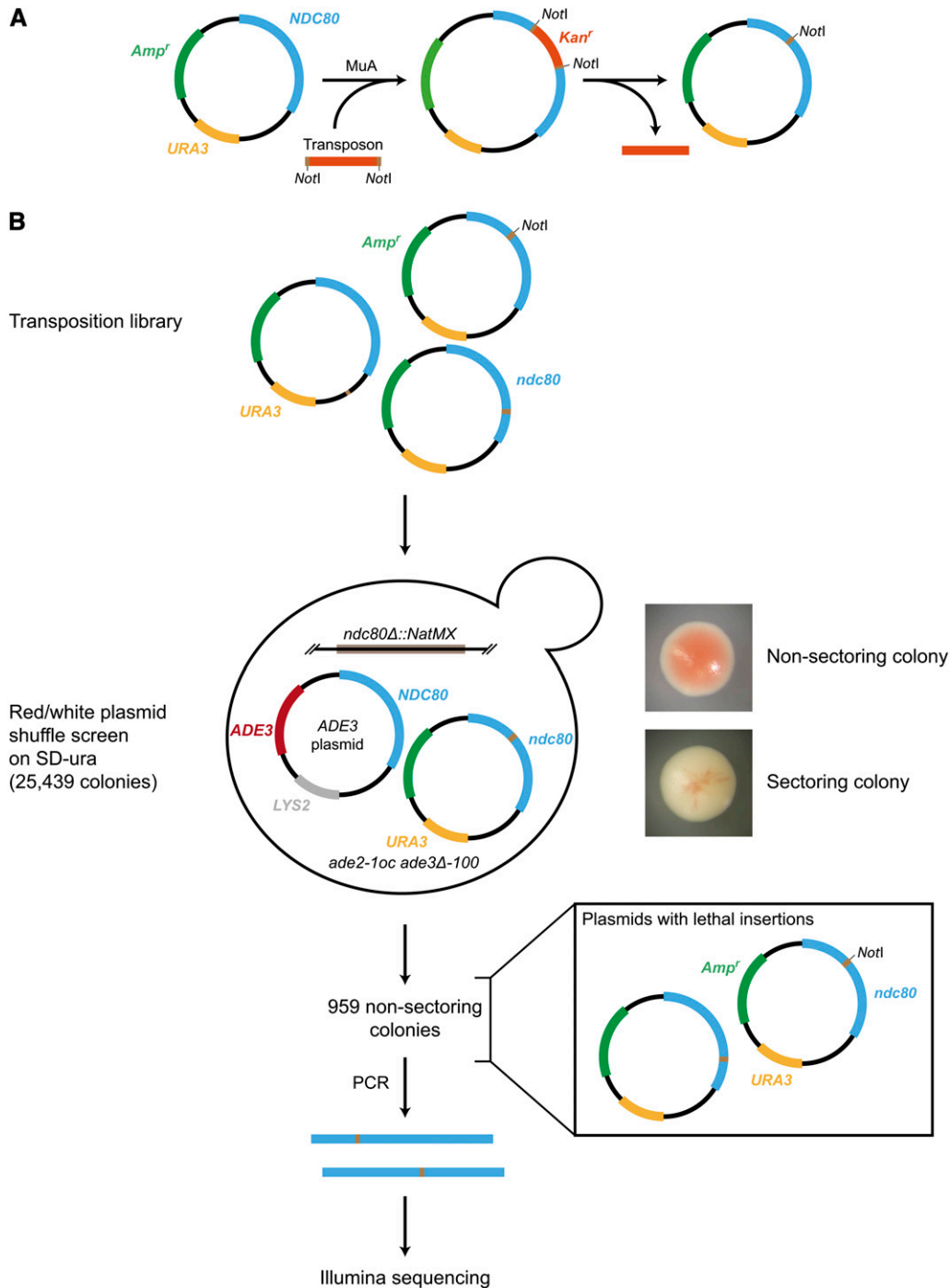


Figure 2 Workflow of the linker-scanning mutagenesis screen. (A) An *Ndc80* transposon library, containing 15-bp insertions at random locations, was created using *MuA* transposition. (B) The transposon library was screened in *S. cerevisiae* using a red/white plasmid shuffle system. Lethal insertions that disrupt the function of *Ndc80* appear as nonsectored red colonies in the screen. From these red colonies, plasmids were isolated and the positions of the lethal insertions were determined by Illumina sequencing.

human crystal structure. The hairpin forms C-terminal to the *Ndc80* CH domain and, together, they “sandwich” the globular domain of *Nuf2* (Ciferri *et al.* 2008). Both of these mutant complexes bound to microtubules *in vitro* (Figure S4). Furthermore, the *ins839* mutation altered the behavior of single molecules of the *Ndc80* complex on microtubules, increasing their residence time and slowing their diffusion as compared to wild type (Figure 4, B and C). This observation suggests that although the hairpin is not part of the microtubule-binding interface, it indirectly affects the attachment between the *Ndc80* complex and microtubules.

The *ins839* *Ndc80* complex is insensitive to the presence of the *Dam1* complex on microtubules

Ndc80 is required for recruitment of the essential *Dam1* complex to kinetochores *in vivo* (Janke *et al.* 2002). *In vitro*, the *Ndc80* and *Dam1* complexes interact directly, in a microtubule-dependent manner (Lampert *et al.* 2010; Tien *et al.* 2010). The *Dam1* complex causes the *Ndc80* complex to dissociate more slowly from microtubules and to diffuse more slowly on the lattice (Tien *et al.* 2010). The *ins839* mutation in the hairpin of *Ndc80* has a similar but less dramatic effect,

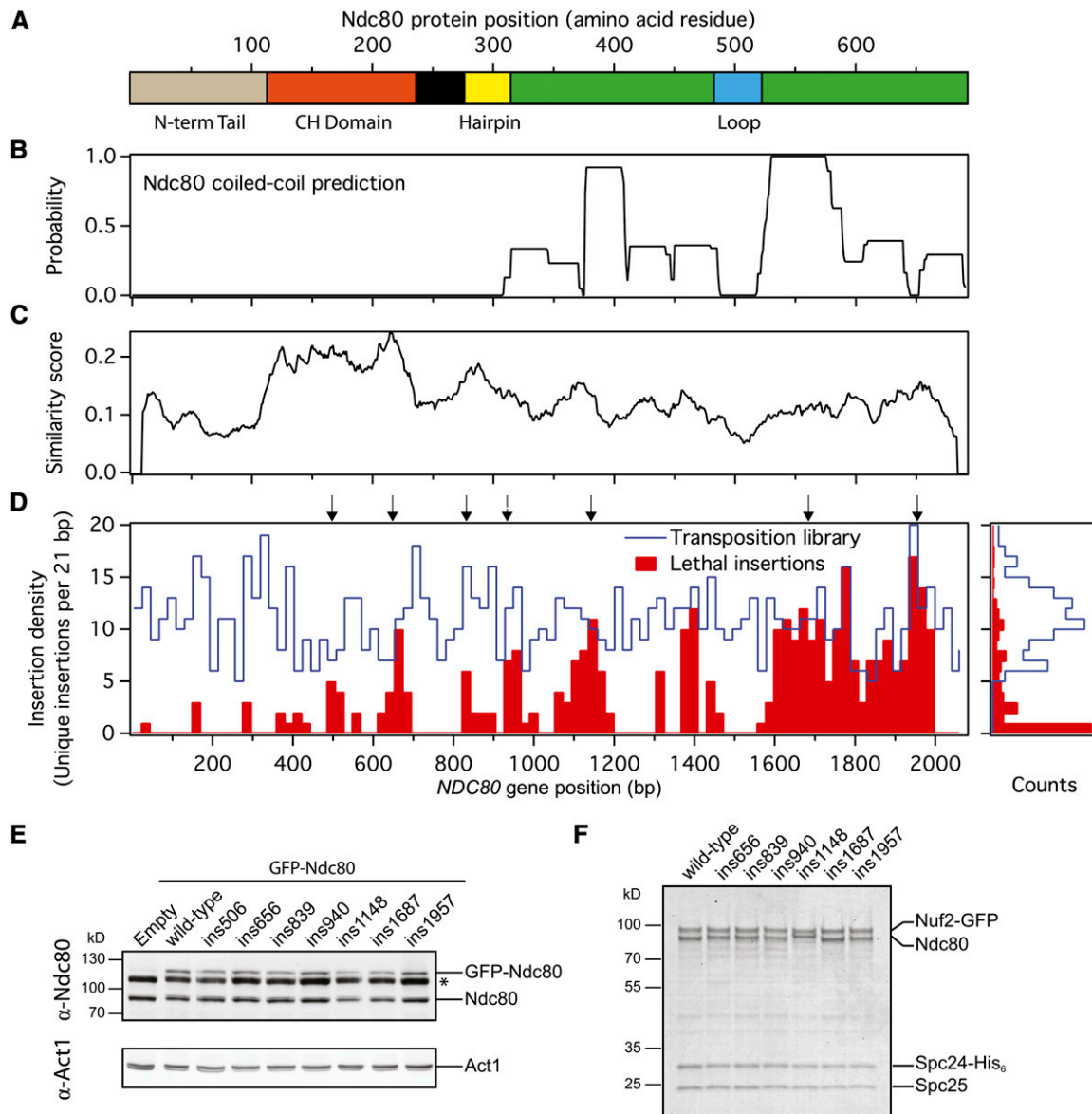


Figure 3 Lethal insertions were found in distinct clusters in *NDC80*. (A) Bar diagram showing the positions of notable structural features in Ndc80. (B) Probability of coiled-coil formation as predicted by Paircoil2 (McDonnell *et al.* 2006). (C) Similarity of Ndc80 protein sequences between select fungal species (see *Materials and Methods*). (D) Left: the insertion density for the transposition library (blue line) and from the red colonies (red bars) is shown along *NDC80*. Insertion density is plotted as the number of unique insertion sites within a 21-bp window. Arrows indicate the positions of the representative insertions characterized. Right: from the insertion density plot, the distributions of insertion densities for the transposition library (blue line) and from the red colonies (red bars) are shown. (E) Immunoblot of cell lysate showing that lethal insertion mutants (GFP tagged) are expressed *in vivo* over the endogenous Ndc80 (untagged). (*) Nonspecific band from the α -Ndc80 antibody. Act1 serves as a loading control. (F) Coomassie-stained gel of recombinant Ndc80 complex containing lethal insertions. Recombinant Ndc80 complexes were purified by affinity chromatography and gel filtration. Mutant Ndc80 complexes migrated similarly to the wild-type complex in the gel filtration column and were collected at the same elution volume. The band for Ndc80 containing the ins1148 mutation reproducibly migrates higher than the wild-type protein.

causing a twofold decrease in the diffusion and dissociation rate constants (Figure 4, B and C). Therefore, we asked whether the *Dam1* complex can further alter the microtubule-binding properties of the *Ndc80* complex with the ins839 mutation. Surprisingly, unlike wild-type *Ndc80* complex and the other five lethal mutant complexes we purified, the ins839 *Ndc80* complex was not influenced by

the presence of the *Dam1* complex (Figure 4, B and C, and Figure S4). Instead, the ins839 mutation makes the *Ndc80* complex insensitive to the presence of the *Dam1* complex. Whether this is a result of the mutation perturbing the microtubule-binding ability of the *Ndc80* complex or disrupting an interaction with the *Dam1* complex remains to be determined (see *Discussion*).

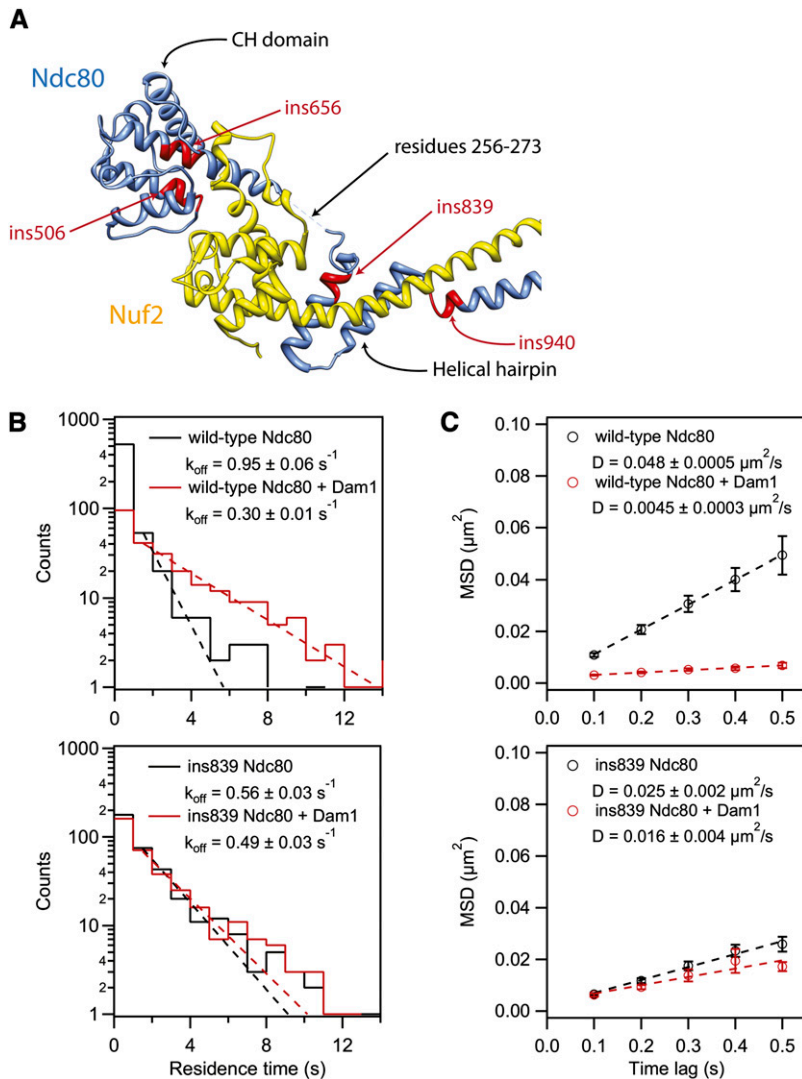


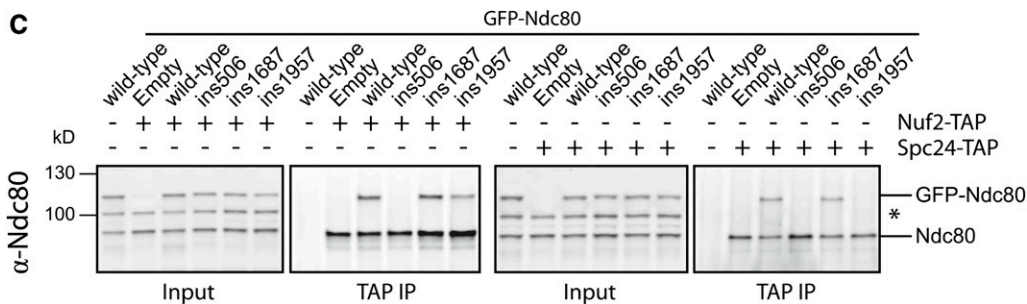
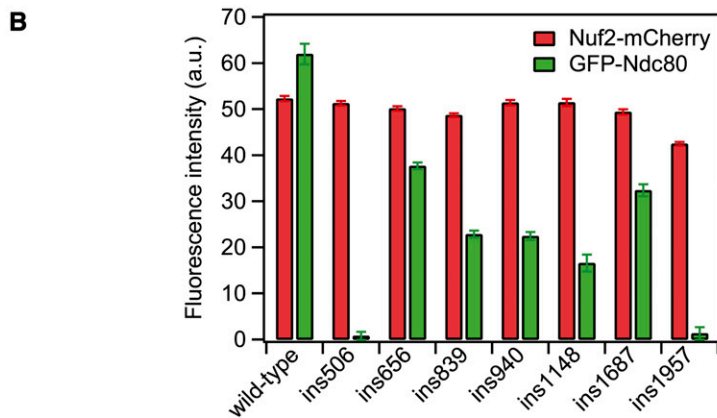
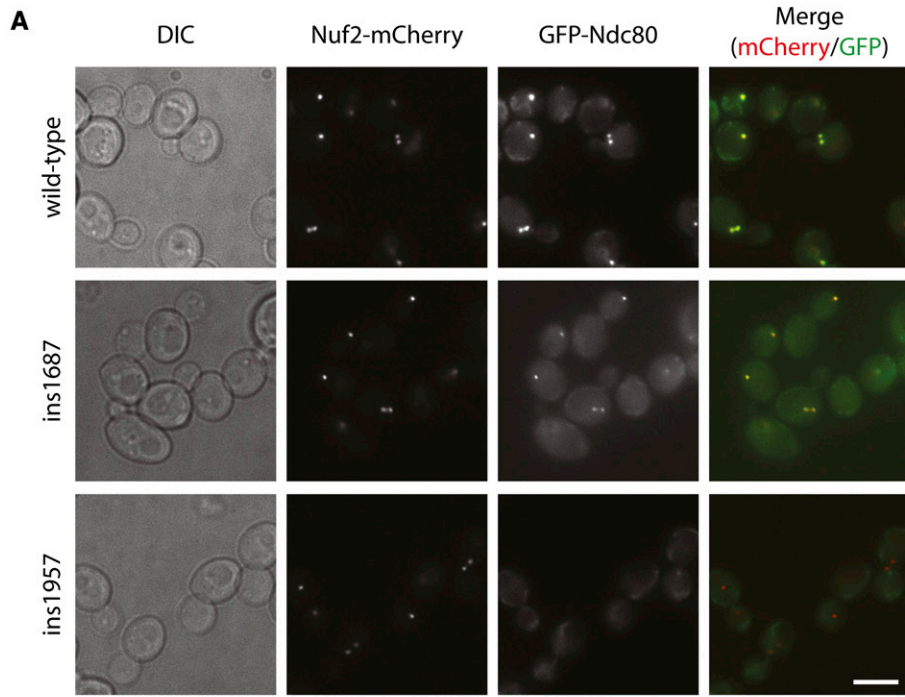
Figure 4 The ability of the Dam1 complex to enhance binding of Ndc80 complexes to microtubules is abrogated by a lethal insertion in the helical hairpin. (A) Four lethal insertion clusters (red) are mapped onto homologous regions of the human Ndc80 (blue) crystal structure (PDB 2VE7; Ciferri *et al.* 2008). Lethal insertion clusters are labeled based on their representative insertion. The structure is illustrated with the UCSF Chimera package (Pettersen *et al.* 2004). (B) Residence time distributions of GFP-tagged Ndc80 complex on microtubules fit with single exponentials (dashed lines) to determine the dissociation rate constants, k_{off} . Top: wild-type Ndc80 complex in the absence (black, $n = 622$) or presence (red, $n = 252$) of Dam1 complex. Bottom: ins839 Ndc80 complex in the absence (black, $n = 374$) or presence (red, $n = 357$) of Dam1 complex. (C) Plots of mean-squared displacement (MSD) \pm SEM vs. time lag for the binding events in B. Linear fits to the data (dashed lines) were used to determine the diffusion constant, D .

The ins1957 mutation in Ndc80 disrupts tetramerization of the Ndc80 complex

Localization of Ndc80 to the kinetochore depends on its assembly into an intact complex with Nuf2, Spc24, and Spc25. This complex is anchored to the kinetochore via interactions between Spc24/Spc25 and other components, such as the Mtw1 complex (De Wulf *et al.* 2003; Maskell *et al.* 2010; Petrovic *et al.* 2010; Hornung *et al.* 2011). From cross-linking and limited proteolysis experiments, it was proposed that the C termini of Ndc80/Nuf2 contact Spc24/Spc25 to assemble the Ndc80 complex (Ciferri *et al.* 2005; Wei *et al.* 2005; Maiolica *et al.* 2007). However, the proteins and residues involved in this putative tetramerization domain and the structural basis for assembly of the complex remain poorly understood.

Our linker-scanning mutagenesis screen identified three previously uncharacterized regions in Ndc80 that are essential for its function (represented by ins1148, ins1687, and ins1957). These regions are C-terminal to the CH domain, and all three representative mutant Ndc80 complexes bound

microtubules similar to the wild-type complex (Figure S4). The ins1687 and ins1957 mutations represent broad, neighboring clusters of lethal insertions that cover an area including the putative tetramerization domain. We screened these and our other representative mutations for defective kinetochore localization of Ndc80. Using fluorescence microscopy, we measured the amount of GFP-tagged mutant Ndc80 that colocalized with Nuf2-mCherry at kinetochores (Figure 5, A and B). The ins656, ins839, ins940, ins1148, and ins1687 mutant GFP-Ndc80 proteins colocalized with Nuf2-mCherry, indicating that these insertions do not disrupt formation of the Ndc80 complex or its association with the kinetochore *in vivo*. By contrast, ins1957 GFP-Ndc80 was absent from kinetochores. Given its position at the C terminus of Ndc80, we hypothesized that the ins1957 mutation disrupts tetramerization of the complex. However, the ins1957 mutant copurifies with Nuf2, Spc24, and Spc25 in a recombinant Ndc80 complex (Figure 3F), suggesting that the mutation does not completely abolish complex formation. To address this question *in vivo*, we performed immunoprecipitation experiments with TAP tags fused to the endogenous Nuf2



or *Spc24* (Figure 5C). We found that ins1957 GFP-Ndc80 co-immunoprecipitated with *Nuf2*-TAP, but not *Spc24*-TAP. As a control, wild-type and ins1687 GFP-Ndc80 co-immunoprecipitated with both *Nuf2*-TAP and *Spc24*-TAP. Consistent with its inability to form a recombinant complex, ins506 GFP-Ndc80 did not interact with *Nuf2*-TAP or *Spc24*-TAP in the co-immunoprecipitation assay and was absent from kinetochores (Figure 5B and C). These results show that

ins506 GFP-Ndc80 cannot pair with *Nuf2* and consequently fails to assemble into an intact complex. By contrast, ins1957 GFP-Ndc80 can pair with *Nuf2* *in vivo*, but is unable to compete with endogenous *Ndc80* for association with *Spc24*/*Spc25* at kinetochores. Therefore, the lethal insertion cluster represented by ins1957 is likely the tetramerization domain, which mediates the association of *Ndc80*/*Nuf2* with *Spc24*/*Spc25* into intact complexes at kinetochores.

Figure 5 A C-terminal segment of *Ndc80* controls tetramerization of the *Ndc80* complex. (A) Sample images of GFP-Ndc80 lethal insertion mutants colocalized with *Nuf2*-mCherry at kinetochores *in vivo*. Endogenous *Ndc80* is untagged. Scale bar, 5 μ m. (B) The fluorescence intensity of GFP and mCherry are quantified and shown. Intensity is plotted as the mean of fluorescence signal—mean of background signal. Error bars represent SEM. The total numbers of mCherry spots quantified are: wild type ($n = 686$), ins506 ($n = 788$), ins656 ($n = 760$), ins839 ($n = 913$), ins940 ($n = 643$), ins1148 ($n = 372$), ins1687 ($n = 576$), and ins1957 ($n = 389$). (C) Immunoprecipitation (IP) of GFP-Ndc80 lethal insertion mutants, and untagged endogenous *Ndc80*, with *Nuf2*-TAP or *Spc24*-TAP. (*) Nonspecific band from the α -*Ndc80* antibody. On the immunoblots, input is 0.5% of the clarified lysate and TAP IP is 10% of the total volume.

Discussion

Linker-scanning mutagenesis specifically identifies regions essential for function

Here, we describe an approach to uncover new functional domains of essential proteins in *S. cerevisiae*. We accomplished this by combining linker-scanning mutagenesis, a plasmid shuffle assay, and high-throughput sequencing together in a comprehensive screen. We applied this screen to the conserved Ndc80 kinetochore protein, which contains a microtubule-binding globular domain and is predicted to contain long coiled-coil domains. While the short insertions resulting from transposon mutagenesis were generally well tolerated, several clusters of insertions were detrimental to Ndc80 function *in vivo*. These clusters of lethal insertions highlight important regions of the protein, many of which are not readily apparent by inspecting sequence conservation (Figure 3C and D).

New functions for the N terminus of Ndc80

Binding of Ndc80 to microtubules is accomplished by its N terminus, which contains an unstructured tail domain and a conserved CH domain that is commonly found on actin- and microtubule-binding proteins (Gimona *et al.* 2002; Korenbaum and Rivero 2002; Hayashi and Ikura 2003; Wei *et al.* 2007; Ciferri *et al.* 2008). In our linker-scanning mutagenesis screen, insertions were generally tolerated throughout the entire N terminus of Ndc80, with just two clusters of lethal insertions in the CH domain. A representative mutation from the first cluster (ins506) is expressed *in vivo*, but is absent from kinetochores and does not co-immunoprecipitate with Nuf2-TAP. This mutant impairs the formation of the Ndc80 complex, likely by disrupting the interaction between the Ndc80 and Nuf2 CH domains. This suggests that the CH domain plays a critical role in the dimerization of Ndc80 and Nuf2. The second cluster lies in an interior helix of the CH domain adjacent to the first cluster. A representative mutation from this cluster (ins656) surprisingly did not abolish microtubule binding by the recombinant complex or disrupt kinetochore localization *in vivo*. It is unlikely that this mutation is lethal because of subtle changes in the microtubule-binding ability of Ndc80, as several mutations that are known to impair microtubule binding by the human complex *in vitro* are tolerated in *S. cerevisiae* (Ciferri *et al.* 2008; Akiyoshi *et al.* 2009; Kemmler *et al.* 2009; Lampert *et al.* 2013; Umbreit *et al.* 2012). We propose that this mutation instead disrupts another essential function of the Ndc80 CH domain that is independent of microtubule binding.

Downstream of the CH domain, we mapped two clusters of lethal insertions to a putative helical hairpin motif. Together with the Ndc80 CH domain, this hairpin packs against the paired CH domain of Nuf2 in a crystal structure of the truncated human Ndc80 complex (Ciferri *et al.* 2008). One of these lethal insertions, ins839, slows the dissociation and diffusion rates of Ndc80 complexes on microtubules *in vitro*. These effects cannot be due to cooperative interactions

between Ndc80 complexes on microtubules, as our experiments were performed at the single-molecule level. Moreover, given its position in the crystal structure, the hairpin is unlikely to contact microtubules directly. Therefore, we propose that the hairpin contributes indirectly to microtubule binding, perhaps through structural stabilization or organization of the microtubule-binding interface.

One key role of Ndc80 *in vivo* is to recruit the Dam1 complex to kinetochores (Janke *et al.* 2002), but the nature of this interaction remains unclear. *In vitro*, the wild-type Ndc80 complex interacts directly with the Dam1 complex in a microtubule-dependent manner (Lampert *et al.* 2010; Tien *et al.* 2010). We found previously that the addition of Dam1 complex decreases the dissociation and diffusion rates of single Ndc80 complexes on microtubules. Here we show that the ins839 mutation parallels these effects on the Ndc80 complex and that the addition of Dam1 complex does not further change the behavior of the ins839 Ndc80 complex on microtubules. Notably, while the dissociation and diffusion rates of single ins839 Ndc80 complexes on microtubules are lower than that of the wild-type complex, they are higher than that of the wild-type complex when assayed in the presence of Dam1 complex. This observation raises the interesting possibility that the Dam1 complex does not simply contribute an additional microtubule-binding domain when it interacts with the Ndc80 complex, but changes how the Ndc80 complex binds to the microtubule lattice. The ins839 mutation could partially mimic this effect, which explains why the mutant Ndc80 complex is not further influenced by the Dam1 complex.

An alternative explanation for our observations is that the ins839 mutation disrupts the interaction interface between Ndc80 and the Dam1 complex. Recent studies have proposed that the Dam1 complex binds directly to Ndc80 within the Ndc80 complex, but did not agree on the location of this interaction interface (Maure *et al.* 2011; Lampert *et al.* 2013). One of these proposed regions, a stretch of Ndc80 between the CH domain and the hairpin (residues 256–273; Figure 4A), lies in close proximity to the ins839 mutation. When this region was deleted, the Dam1 complex did not enhance the cosedimentation of the mutant complex with microtubules *in vitro* (Lampert *et al.* 2013). The authors concluded that residues 256–273 represent an interaction interface between Ndc80 and the Dam1 complex. However, like the ins839 mutation, a deletion of this region alters the microtubule-binding behavior of the Ndc80 complex alone (Lampert *et al.* 2013). Therefore, it remains unclear whether these mutations directly disrupt the Dam1 binding interface, or if microtubule attachments made by the mutant complexes are simply unable to be strengthened by the Dam1 complex. Future studies will be aimed at determining whether this region of Ndc80 is in direct contact with the Dam1 complex.

Identification of novel domains in Ndc80 and defining the tetramerization domain

Our linker-scanning mutagenesis screen successfully identified three previously uncharacterized segments of Ndc80 as

regions essential for its function *in vivo*. These three lethal insertion clusters lie in the last ~300 amino acid residues of Ndc80, predicted to form the “rod-shaped” part of the complex as seen by electron microscopy (Wei *et al.* 2005; Wang *et al.* 2008). The first cluster is centered on residue K380 of Ndc80, and coincides with a change in predicted coiled-coil character that may represent a transition point where the coiled-coil begins. Consistent with this prediction, limited proteolysis experiments identified K380 as a cleavage site that is likely unprotected by coiled-coil (Wei *et al.* 2005). The representative insertion from this cluster, ins1148, is predicted to abolish the formation of coiled coil after the insertion (Figure S5). Nevertheless it forms a stable tetramer both *in vivo* and *in vitro*, suggesting the coiled coil in this region is not driving the interaction between Ndc80 and Nuf2, Spc24, or Spc25. Similarly the cluster represented by ins1687 abolishes the probability of coiled-coil formation after this insertion, but again has no effect on tetramer formation and represents a domain with an, as yet, unknown function.

The cluster represented by ins1957 is in a region predicted to overlap with the N termini of Spc24/Spc25 by crosslinking experiments (Maiolica *et al.* 2007). While this general region is proposed to mediate tetramerization of the complex (Ciferri *et al.* 2005; Wei *et al.* 2005; Maiolica *et al.* 2007), it is not clear which complex components are directly involved and which segments of these components are required. We found that the ins1957 mutation disrupts formation of the Ndc80 complex *in vivo* and that the mutant Ndc80 was consequently defective at incorporating into kinetochores. These results suggest that the lethal insertion cluster represented by the ins1957 mutation defines a region in Ndc80 important for tetramerization of the Ndc80 complex.

Using the linker-scanning mutagenesis screen, we have identified lethal insertions in known structural elements of Ndc80 and, additionally, defined new functional domains in the protein. Future experiments will examine individual domains with the goal of defining binding interfaces with known partners, searching for novel protein interactions, and uncovering new roles for Ndc80. This approach is generally applicable to other genes in *S. cerevisiae* and is particularly useful in revealing functional properties and domains in proteins that are not yet amenable to structural characterization.

Acknowledgments

We thank members of the Davis Lab and the Seattle Mitosis group for helpful discussions. We also thank I. Onn, D. Koshland, C. Lee, and J. Shendure for technical assistance and A. Desai for the α -Ndc80 antibody. This work was supported by a National Sciences and Engineering Research Council of Canada scholarship (to J.F.T.), National Institutes of Health Grants T32 GM008268 (to N.T.U.) and T32 GM007270 (to K.K.F.), Searle Scholar Award Grant 06-L-111 (to C.L.A.), Packard Fellowship for Science and Engineering

Grant 2006-30521 (to C.L.A.), National Center for Research Resources Grant S10 RR26406 (to C.L.A.), and National Institute of General Medical Sciences Grants R01 GM40506 (to T.N.D.) and R01 GM079373 (to C.L.A.). M.J.D. is funded by the National Institute of General Medical Sciences Grant P41 GM103533 to T.N.D. M.J.D. is a Rita Allen Scholar.

Literature Cited

- Akiyoshi, B., C. R. Nelson, J. A. Ranish, and S. Biggins, 2009 Analysis of Ipl1-mediated phosphorylation of the Ndc80 kinetochore protein in *Saccharomyces cerevisiae*. *Genetics* 183: 1591–1595.
- Alushin, G. M., V. H. Ramey, S. Pasqualato, D. A. Ball, N. Grigorieff *et al.*, 2010 The Ndc80 kinetochore complex forms oligomeric arrays along microtubules. *Nature* 467: 805–810.
- Asbury, C. L., D. R. Gestaut, A. F. Powers, A. D. Franck, and T. N. Davis, 2006 The Dam1 kinetochore complex harnesses microtubule dynamics to produce force and movement. *Proc. Natl. Acad. Sci. USA* 103: 9873–9878.
- Bender, A., and J. R. Pringle, 1991 Use of a screen for synthetic lethal and multicopy suppressor mutants to identify two new genes involved in morphogenesis in *Saccharomyces cerevisiae*. *Mol. Cell. Biol.* 11: 1295–1305.
- Blackshields, G., F. Sievers, W. Shi, A. Wilm, and D. G. Higgins, 2010 Sequence embedding for fast construction of guide trees for multiple sequence alignment. *Algorithms Mol. Biol.* 5: 21.
- Burke, D., D. Dawson, and T. Stearns, 2000 *Methods in Yeast Genetics*. Cold Spring Harbor Laboratory Press, Cold Spring Harbor, NY.
- Ciferri, C., J. De Luca, S. Monzani, K. J. Ferrari, D. Ristic *et al.*, 2005 Architecture of the human ndc80-hec1 complex, a critical constituent of the outer kinetochore. *J. Biol. Chem.* 280: 29088–29095.
- Ciferri, C., S. Pasqualato, E. Screpanti, G. Varetto, S. Santaguida *et al.*, 2008 Implications for kinetochore-microtubule attachment from the structure of an engineered Ndc80 complex. *Cell* 133: 427–439.
- Davis, T. N., 1992 Mutational analysis of calmodulin in *Saccharomyces cerevisiae*. *Cell Calcium* 13: 435–444.
- DeLuca, K. F., S. M. Lens, and J. G. DeLuca, 2011 Temporal changes in Hec1 phosphorylation control kinetochore-microtubule attachment stability during mitosis. *J. Cell Sci.* 124: 622–634.
- De Wulf, P., A. D. McAinsh, and P. K. Sorger, 2003 Hierarchical assembly of the budding yeast kinetochore from multiple sub-complexes. *Genes Dev.* 17: 2902–2921.
- Gimona, M., K. Djinovic-Carugo, W. J. Kranewitter, and S. J. Winder, 2002 Functional plasticity of CH domains. *FEBS Lett.* 513: 98–106.
- Guimaraes, G. J., Y. Dong, B. F. McEwen, and J. G. DeLuca, 2008 Kinetochore-microtubule attachment relies on the disordered N-terminal tail domain of Hec1. *Curr. Biol.* 18: 1778–1784.
- Hach, F., F. Hormozdiari, C. Alkan, I. Birol, E. E. Eichler *et al.*, 2010 mrsFAST: a cache-oblivious algorithm for short-read mapping. *Nat. Methods* 7: 576–577.
- Hayashi, I., and M. Ikura, 2003 Crystal structure of the amino-terminal microtubule-binding domain of end-binding protein 1 (EB1). *J. Biol. Chem.* 278: 36430–36434.
- He, X., D. R. Rines, C. W. Espelin, and P. K. Sorger, 2001 Molecular analysis of kinetochore-microtubule attachment in budding yeast. *Cell* 106: 195–206.
- Hornung, P., M. Maier, G. M. Alushin, G. C. Lander, E. Nogales *et al.*, 2011 Molecular architecture and connectivity of the budding yeast Mtw1 kinetochore complex. *J. Mol. Biol.* 405: 548–559.

- Janke, C., J. Ortiz, J. Lechner, A. Shevchenko, M. M. Magiera *et al.*, 2001 The budding yeast proteins Spc24p and Spc25p interact with Ndc80p and Nuf2p at the kinetochore and are important for kinetochore clustering and checkpoint control. *EMBO J.* 20: 777–791.
- Janke, C., J. Ortiz, T. U. Tanaka, J. Lechner, and E. Schiebel, 2002 Four new subunits of the Dam1–Duo1 complex reveal novel functions in sister kinetochore biorientation. *EMBO J.* 21: 181–193.
- Kemmler, S., M. Stach, M. Knapp, J. Ortiz, J. Pfannstiel *et al.*, 2009 Mimicking Ndc80 phosphorylation triggers spindle assembly checkpoint signalling. *EMBO J.* 28: 1099–1110.
- Kline-Smith, S. L., S. Sandall, and A. Desai, 2005 Kinetochore-spindle microtubule interactions during mitosis. *Curr. Opin. Cell Biol.* 17: 35–46.
- Korenbaum, E., and F. Rivero, 2002 Calponin homology domains at a glance. *J. Cell Sci.* 115: 3543–3545.
- Lampert, F., P. Hornung, and S. Westermann, 2010 The Dam1 complex confers microtubule plus end-tracking activity to the Ndc80 kinetochore complex. *J. Cell Biol.* 189: 641–649.
- Lampert, F., C. Mieck, G. M. Alushin, E. Nogales, and S. Westermann, 2013 Molecular requirements for the formation of a kinetochore-microtubule interface by Dam1 and Ndc80 complexes. *J. Cell Biol.* 200: 21–30.
- Maiolica, A., D. Cittaro, D. Borsotti, L. Sennels, C. Ciferri *et al.*, 2007 Structural analysis of multiprotein complexes by cross-linking, mass spectrometry, and database searching. *Mol. Cell. Proteomics* 6: 2200–2211.
- Malvezzi, F., G. Litos, A. Schleiffer, A. Heuck, K. Mechtler *et al.*, 2013 A structural basis for kinetochore recruitment of the Ndc80 complex via two distinct centromere receptors. *EMBO J.* 32: 409–423.
- Maskell, D. P., X. W. Hu, and M. R. Singleton, 2010 Molecular architecture and assembly of the yeast kinetochore MIND complex. *J. Cell Biol.* 190: 823–834.
- Maure, J. F., S. Komoto, Y. Oku, A. Mino, S. Pasqualato *et al.*, 2011 The Ndc80 loop region facilitates formation of kinetochore attachment to the dynamic microtubule plus end. *Curr. Biol.* 21: 207–213.
- McDonnell, A. V., T. Jiang, A. E. Keating, and B. Berger, 2006 Paircoil2: improved prediction of coiled coils from sequence. *Bioinformatics* 22: 356–358.
- Miller, S. A., M. L. Johnson, and P. T. Stukenberg, 2008 Kinetochore attachments require an interaction between unstructured tails on microtubules and Ndc80(Hec1). *Curr. Biol.* 18: 1785–1791.
- Milutinovich, M., E. Unal, C. Ward, R. V. Skibbens, and D. Koshland, 2007 A multi-step pathway for the establishment of sister chromatid cohesion. *PLoS Genet.* 3: e12.
- Miranda, J. J., P. De Wulf, P. K. Sorger, and S. C. Harrison, 2005 The yeast DASH complex forms closed rings on microtubules. *Nat. Struct. Mol. Biol.* 12: 138–143.
- Muller, E. G., 1996 A glutathione reductase mutant of yeast accumulates high levels of oxidized glutathione and requires thioredoxin for growth. *Mol. Biol. Cell* 7: 1805–1813.
- Muller, E. G. D., B. E. Snyderman, I. Novik, D. W. Hailey, D. R. Gestaut *et al.*, 2005 The organization of the core proteins of the yeast spindle pole body. *Mol. Biol. Cell* 16: 3341–3352.
- Nguyen, T., D. B. N. Vinh, D. K. Crawford, and T. N. Davis, 1998 A genetic analysis of interactions with Spc110p reveals distinct functions of Spc97p and Spc98p, components of the yeast gamma-tubulin complex. *Mol. Biol. Cell* 9: 2201–2216.
- Nishino, T., F. Rago, T. Hori, K. Tomii, I. M. Cheeseman *et al.*, 2013 CENP-T provides a structural platform for outer kinetochore assembly. *EMBO J.* 32: 424–436.
- Osborne, M. A., G. Schlenstedt, T. Jinks, and P. A. Silver, 1994 Nuf2, a spindle pole body-associated protein required for nuclear division in yeast. *J. Cell Biol.* 125: 853–866.
- Pajunen, M., H. Turakainen, E. Poussu, J. Peranen, M. Vihinen *et al.*, 2007 High-precision mapping of protein-protein interfaces: an integrated genetic strategy combining en masse mutagenesis and DNA-level parallel analysis on a yeast two-hybrid platform. *Nucleic Acids Res.* 35: e103.
- Petrovic, A., S. Pasqualato, P. Dube, V. Krenn, S. Santaguida *et al.*, 2010 The MIS12 complex is a protein interaction hub for outer kinetochore assembly. *J. Cell Biol.* 190: 835–852.
- Pettersen, E. F., T. D. Goddard, C. C. Huang, G. S. Couch, D. M. Greenblatt *et al.*, 2004 UCSF Chimera: a visualization system for exploratory research and analysis. *J. Comput. Chem.* 25: 1605–1612.
- Petyuk, V., J. McDermott, M. Cook, and B. Sauer, 2004 Functional mapping of Cre recombinase by pentapeptide insertional mutagenesis. *J. Biol. Chem.* 279: 37040–37048.
- Powers, A. F., A. D. Franck, D. R. Gestaut, J. Cooper, B. Graczyk *et al.*, 2009 The Ndc80 kinetochore complex forms load-bearing attachments to dynamic microtubule tips via biased diffusion. *Cell* 136: 865–875.
- Rice, P., I. Longden, and A. Bleasby, 2000 EMBOSS: the European Molecular Biology Open Software Suite. *Trends Genet.* 16: 276–277.
- Scannell, D. R., O. A. Zill, A. Rokas, C. Payen, M. J. Dunham *et al.*, 2011 The awesome power of yeast evolutionary genetics: new genome sequences and strain resources for the *Saccharomyces sensu stricto* genus. *G3: Genes, Genomes, Genetics* 1: 11–25.
- Schmidt, J. C., H. Arthanari, A. Boeszoermyenyi, N. M. Dashkevich, E. M. Wilson-Kubalek *et al.*, 2012 The kinetochore-bound Ska1 complex tracks depolymerizing microtubules and binds to curved protofilaments. *Dev. Cell* 23: 968–980.
- Shimogawa, M. M., M. M. Wargacki, E. G. Muller, and T. N. Davis, 2010 Laterally attached kinetochores recruit the checkpoint protein Bub1, but satisfy the spindle checkpoint. *Cell Cycle* 9: 3619–3628.
- Tien, J. F., N. T. Umbreit, D. R. Gestaut, A. D. Franck, J. Cooper *et al.*, 2010 Cooperation of the Dam1 and Ndc80 kinetochore complexes enhances microtubule coupling and is regulated by aurora B. *J. Cell Biol.* 189: 713–723.
- Umbreit, N. T., D. R. Gestaut, J. F. Tien, B. S. Vollmar, T. Gonen *et al.*, 2012 The Ndc80 kinetochore complex directly modulates microtubule dynamics. *Proc. Natl. Acad. Sci. USA* 109: 16113–16118.
- Wang, H. W., S. Long, C. Ciferri, S. Westermann, D. Drubin *et al.*, 2008 Architecture and flexibility of the yeast Ndc80 kinetochore complex. *J. Mol. Biol.* 383: 894–903.
- Wei, R. R., P. K. Sorger, and S. C. Harrison, 2005 Molecular organization of the Ndc80 complex, an essential kinetochore component. *Proc. Natl. Acad. Sci. USA* 102: 5363–5367.
- Wei, R. R., J. R. Schnell, N. A. Larsen, P. K. Sorger, J. J. Chou *et al.*, 2006 Structure of a central component of the yeast kinetochore: the Spc24p/Sp25p globular domain. *Structure* 14: 1003–1009.
- Wei, R. R., J. Al-Bassam, and S. C. Harrison, 2007 The Ndc80/HEC1 complex is a contact point for kinetochore-microtubule attachment. *Nat. Struct. Mol. Biol.* 14: 54–59.
- Wigge, P. A., and J. V. Kilmartin, 2001 The Ndc80p complex from *Saccharomyces cerevisiae* contains conserved centromere components and has a function in chromosome segregation. *J. Cell Biol.* 152: 349–360.
- Wigge, P. A., O. N. Jensen, S. Holmes, S. Soues, M. Mann *et al.*, 1998 Analysis of the *Saccharomyces* spindle pole by matrix-assisted laser desorption/ionization (MALDI) mass spectrometry. *J. Cell Biol.* 141: 967–977.

Communicating editor: O. Cohen-Fix

GENETICS

Supporting Information

<http://www.genetics.org/lookup/suppl/doi:10.1534/genetics.113.152728/-/DC1>

Coupling Unbiased Mutagenesis to High-throughput DNA Sequencing Uncovers Functional Domains in the Ndc80 Kinetochores Protein of *Saccharomyces cerevisiae*

Jerry F. Tien, Kimberly K. Fong, Neil T. Umbreit, Celia Payen, Alex Zelter, Charles L. Asbury,
Maitreya J. Dunham, and Trisha N. Davis

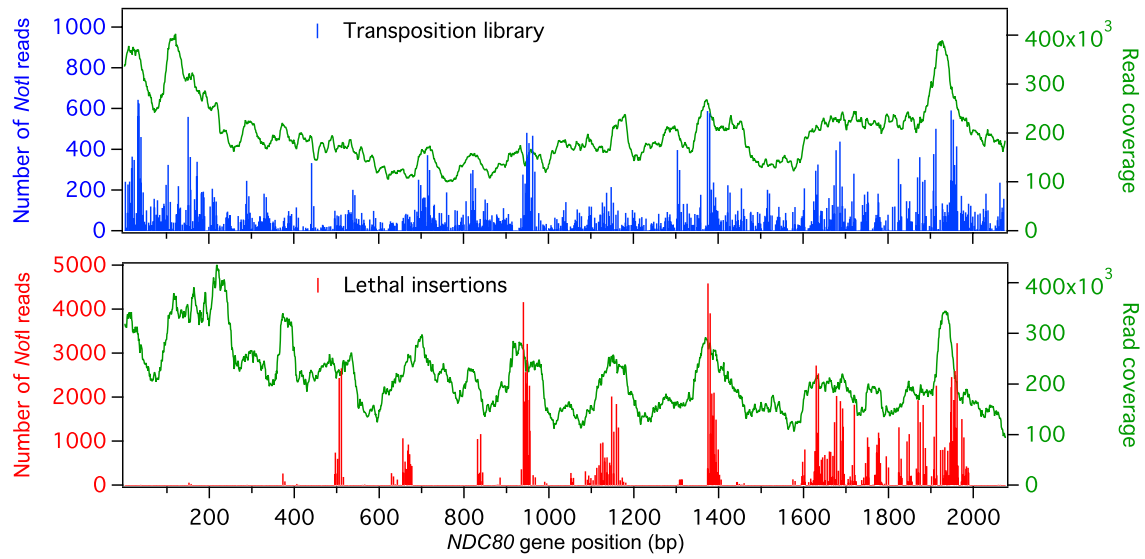


Figure S1 Positions of 15-bp insertions in the transposition library (blue lines) and from the non-sectored red colonies (red lines) were determined by Illumina sequencing. Insertions were identified using the unique *NotI* recognition sequence and shown along the *NDC80* gene. The read coverage from the sequencing is shown in green.

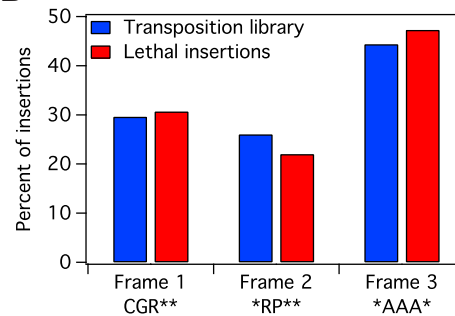
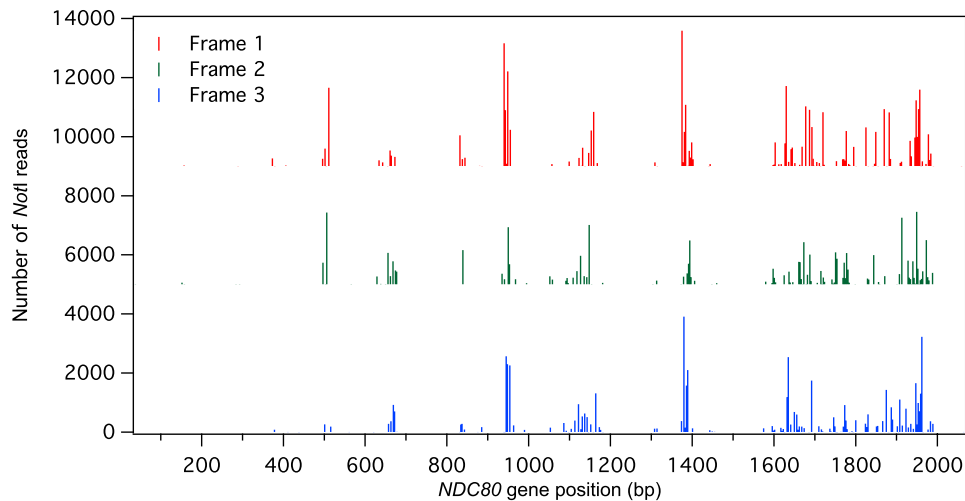
A**Original:** 5' - NNN12345NNN - 3'**Frame 1:** 5' - N12 345 TGC GGC CGC A12 345 NNN - 3'
X X Cys Gly Arg X¹ X X**Frame 2:** 5' - NN1 234 5TG CGG CCG CA1 234 5NN - 3'
X X Leu Arg Pro His X X
Met Gln
Val**Frame 3:** 5' - NNN 123 45T GCG GCC GCA 123 45N - 3'
X X X² Ala Ala Ala X X**Example insertion:****Original:** 5' - CAA**GTGGT**TAT - 3'**Frame 1:** 5' - **AGT GGT TGC GGC CGC AGT GGT** TAT - 3'
Ser Gly Cys Gly Arg Ser Gly Tyr**Frame 2:** 5' - AAG **TGG TTG CGG CCG CAG TGG** TTA - 3'
Lys Trp Leu Arg Pro Gln Trp Leu**Frame 3:** 5' - CAA **GTG GTT GCG GCC GCA GTG GTT** - 3'
Gln Val Val Ala Ala Ala Val Val**B****C**

Figure S2 The reading frame targeted by transposition dictates the residues inserted. (A) The translation of the insertion depends on both the frame of insertion and the target sequence (adapted from Finnzymes Manual F-701). In the transposition library, each 15-bp insertion includes 5 bp of duplicated target sequence (red) and 10 additional nucleotides (blue). X is any amino acid; X¹ is Ile, Met, Thr, Asn, Lys, Ser, or Arg; X² is any amino acid except Gln, Glu, Lys, Met, and Trp. An example insertion is also shown. (B) The proportion of lethal insertions in each frame (red) is similar to that of the initial transposition library (blue). (C) The positions of lethal insertions (from Figure S1) are separated based on the frame of insertion. Traces are offset vertically for visual clarity.

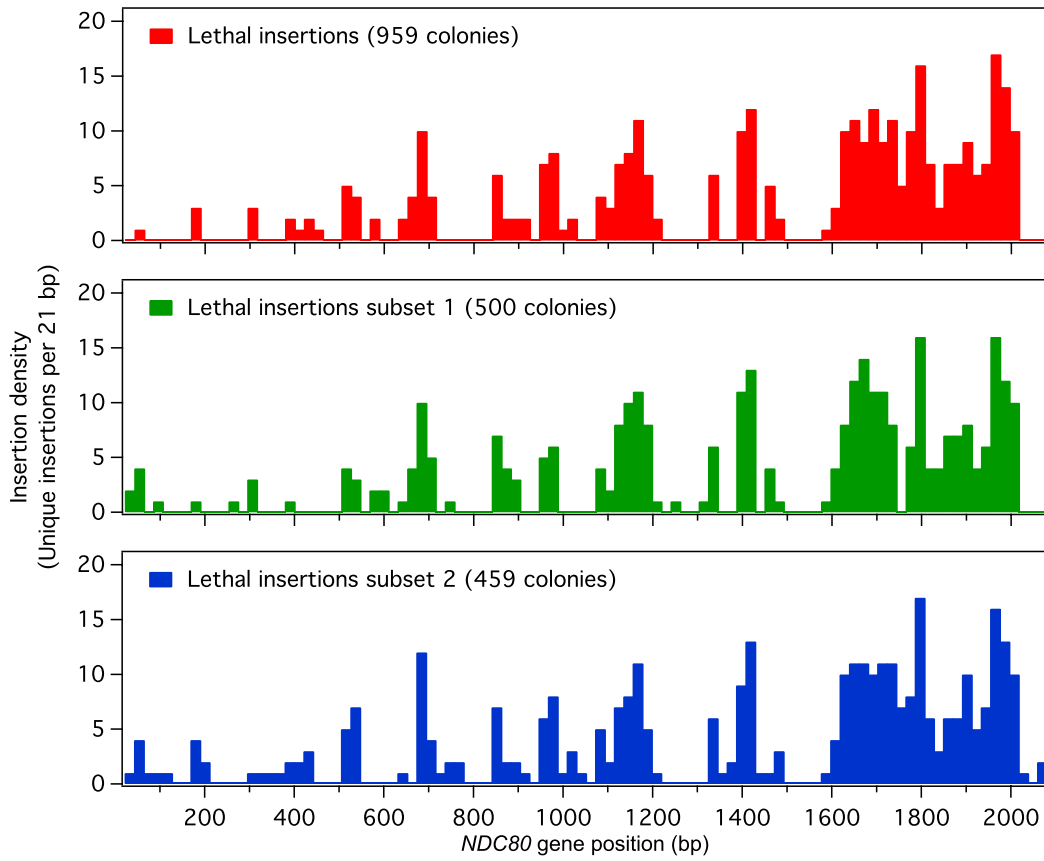


Figure S3 Validation of the lethal insertion clusters. Two subsets (green and blue bars) sequenced independently have the same lethal insertion clusters as the original 959 non-sectoring red colonies (red bars, from Figure 3D).

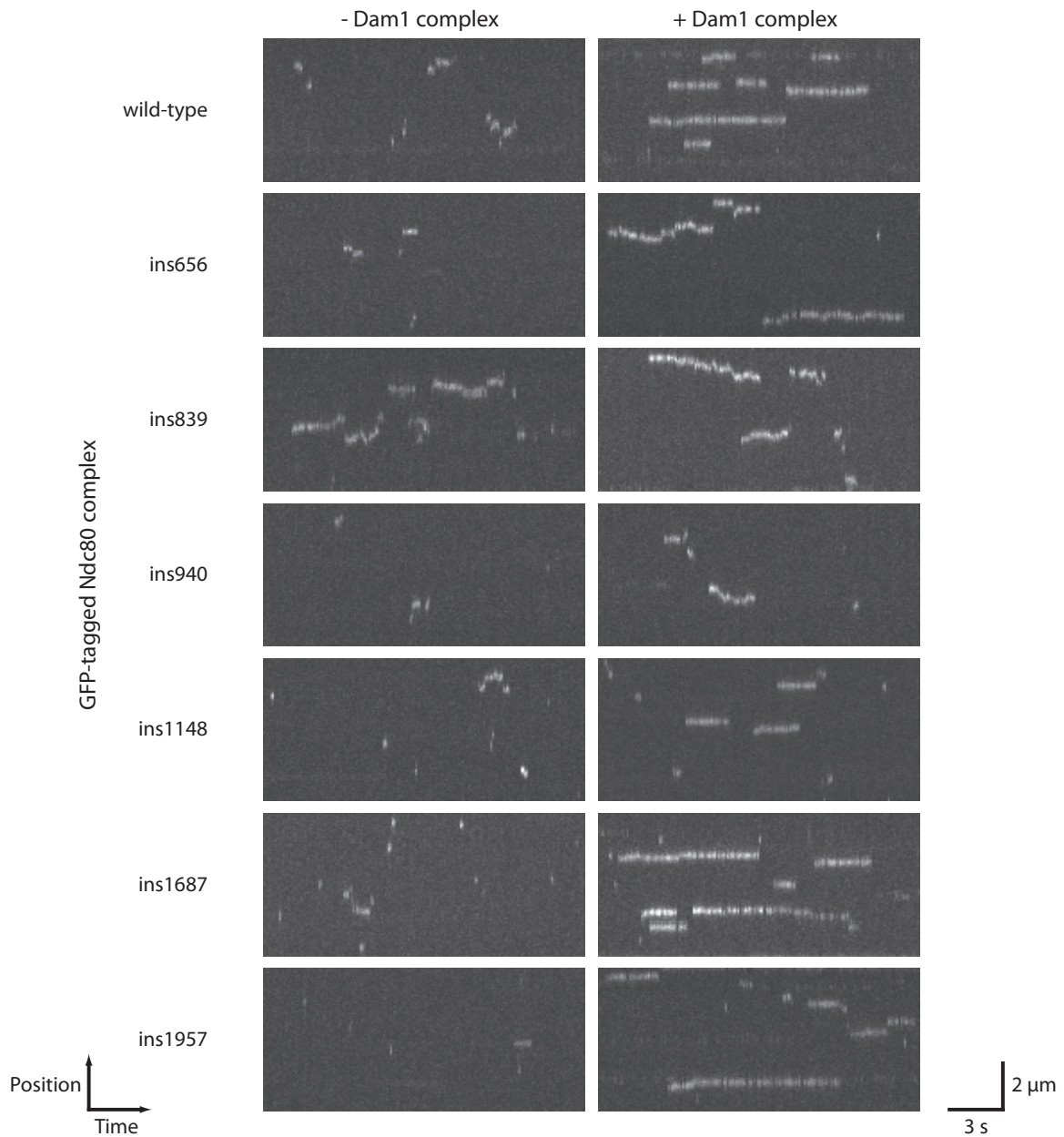


Figure S4 Lethal insertion mutants affect the ability of the Dam1 complex to enhance binding of the Ndc80 complex to microtubules. Using TIRF microscopy, single molecules of GFP-tagged Ndc80 complexes were visualized on taxol-stabilized microtubules. Representative kymographs show the binding and one-dimensional diffusion of 50 pM GFP-tagged Ndc80 complexes on microtubules in the presence or absence of 2.5 nM untagged Dam1 complex.

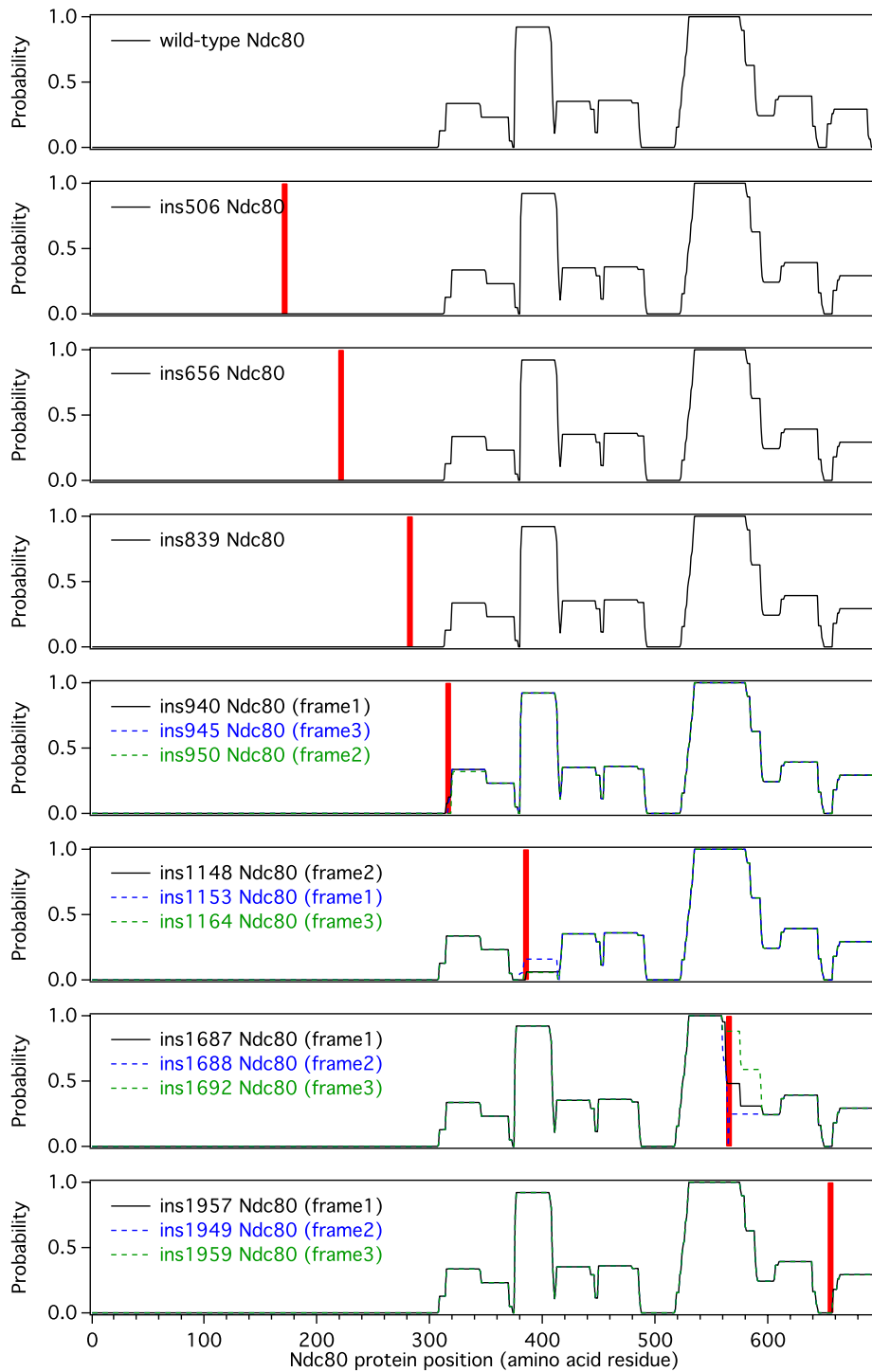


Figure S5 The effect of lethal insertions in Ndc80 on predicted coiled-coil formation. The probabilities of coiled-coil formation, as predicted by Paircoil2 (McDONNELL *et al.* 2006), for Ndc80 containing the representative lethal insertions studied (black lines). Vertical red lines denote the positions of the representative insertions. The probabilities of coiled-coil formation for additional lethal insertions are also shown (blue and green dotted lines).

Table S1 Plasmids used in this study

Plasmid	Relevant markers	Reference
pRS316	<i>CEN6 ARSH4 URA3 Amp^r f1 origin</i>	SIKORSKI and HIETER 1989
pKG9	<i>NatMX</i>	GREENLAND <i>et al.</i> 2010
pJT12	<i>NDC80 ADE3 LYS2</i> in 2 μ m vector	This study
pJT36	<i>NDC80</i> in pRS316	This study
pJT153	<i>GFP-NDC80</i> in pRS316	This study
pJT185	<i>ins506 GFP-ndc80</i> in pRS316	This study
pJT187	<i>ins656 GFP-ndc80</i> in pRS316	This study
pJT188	<i>ins839 GFP-ndc80</i> in pRS316	This study
pJT189	<i>ins940 GFP-ndc80</i> in pRS316	This study
pJT190	<i>ins1148 GFP-ndc80</i> in pRS316	This study
pJT154	<i>ins1687 GFP-ndc80</i> in pRS316	This study
pJT155	<i>ins1957 GFP-ndc80</i> in pRS316	This study
His ₆ -Spc24/Spc25 expression plasmid	<i>His₆-SPC24/SPC25</i> dicistron, <i>Kan^r</i>	WEI <i>et al.</i> 2005
Ndc80/Nuf2-GFP expression plasmid	<i>NDC80/NUF2-GFP</i> dicistron, <i>Amp^r</i>	POWERS <i>et al.</i> 2009
pJT138	<i>ins506 ndc80/NUF2-GFP</i> dicistron, <i>Amp^r</i>	This study
pJT139	<i>ins511 ndc80/NUF2-GFP</i> dicistron, <i>Amp^r</i>	This study
pJT140	<i>ins656 ndc80/NUF2-GFP</i> dicistron, <i>Amp^r</i>	This study
pJT141	<i>ins839 ndc80/NUF2-GFP</i> dicistron, <i>Amp^r</i>	This study
pJT142	<i>ins940 ndc80/NUF2-GFP</i> dicistron, <i>Amp^r</i>	This study
pJT143	<i>ins1148 ndc80/NUF2-GFP</i> dicistron, <i>Amp^r</i>	This study
pJT145	<i>ins1687 ndc80/NUF2-GFP</i> dicistron, <i>Amp^r</i>	This study
pJT146	<i>ins1957 ndc80/NUF2-GFP</i> dicistron, <i>Amp^r</i>	This study
Dam1 complex expression plasmid	<i>DAD4/DAD3/DAD2/SPC19/ASK1</i> and <i>DAD1/DUO1/SPC34-His₆/DAM1/HSK3</i> polycistrons, <i>Amp^r</i>	MIRANDA <i>et al.</i> 2005

Table S2 Yeast strains used in this study

Strain	Genotype	Reference
W303	<i>ade2-1oc can1-100 his3-11,15 leu2-3,112 trp1-1 ura3-1</i>	
JTY1	<i>MATa/α ade2-1oc/ade2-1oc ade3Δ-100/ade3Δ-100 can1-100/can1-100 cyh2^f/CYH2^s his3-11,15/his3-11,15 leu2-3,112/leu2-3,112 lys2Δ::HIS3/lys2Δ::HIS3 trp1-1/trp1-1 ura3-1/ura3-1</i>	This study
JTY4	<i>MATa/α ade2-1oc/ade2-1oc ade3Δ-100/ade3Δ-100 can1-100/can1-100 cyh2^f/CYH2^s his3-11,15/his3-11,15 leu2-3,112/leu2-3,112 lys2Δ::HIS3/lys2Δ::HIS3 trp1-1/trp1-1 ura3-1/ura3-1 NDC80/ndc80Δ::NatMX</i>	This study
JTY5-5C	<i>MATa ade2-1oc ade3Δ-100 can1-100 cyh2^f his3-11,15 leu2-3,112 lys2Δ::HIS3 trp1-1 ura3-1 ndc80Δ::NatMX [pJT12]</i>	This study
JTY12-25A	<i>MATa ade2-1oc ade3Δ-100 can1-100 cyh2^f his3-11,15 leu2-3,112 trp1-1 ura3-1 NDC80 NUF2-mCherry::hphMX</i>	This study
JTY29-1B	<i>MATα ade2-1oc ade3Δ-100 can1-100 cyh2^f his3-11,15 leu2-3,112 trp1-1 ura3-1 NUF2</i>	This study
JTY29-1C	<i>MATα ade2-1oc ade3Δ-100 can1-100 CYH2^s his3-11,15 leu2-3,112 trp1-1 ura3-1 NUF2-TAP::KanMX</i>	This study
JTY47-2A	<i>MATa ade2-1oc ade3Δ-100 can1-100 CYH2^s his3-11,15 leu2-3,112 trp1-1 ura3-1 SPC24</i>	This study
JTY47-2B	<i>MATα ade2-1oc ade3Δ-100 can1-100 cyh2^f his3-11,15 leu2-3,112 trp1-1 ura3-1 SPC24-TAP::KanMX</i>	This study

Table S3 Oligonucleotides used for Illumina sequencing

Primer	Sequence
<i>NDC80</i> forward PCR primer	TAAAGGGAACAAAAGCTGGG
<i>NDC80</i> reverse PCR primer	ACGCCAGTGAATTGTAA
Multiplex adapter 1	5' P-GATCGGAAGAGCACACGTCT
Multiplex adapter 2	ACACTCTTCCCTACACGACGCTCTCCGATCT
Multiplex forward PCR primer + index 1	AATGATACGGCGACCACCGCATCTCGTGATACACTCTTCCCTACACGACGCTCTCCGATC
Multiplex forward PCR primer + index 2	AATGATACGGCGACCACCGCATCTACATCGACACTCTTCCCTACACGACGCTCTCCGATC
Multiplex reverse PCR primer	CAAGCAGAAGACGGCATACGAGATACACTCTTCCCTACACGACGCTCTCCGATCT
Multiplex index sequencing primer	AGATCGGAAGAGCGTCGTGTAGGGAAAGAGTGT
Multiplex read1 sequencing primer	ACACTCTTCCCTACACGACGCTCTCCGATCT
TruSeq Indexed Adapter AD002	GATCGGAAGAGCACACGTCTGAACTCCAGTCACCGATGTATCTCGTATGCCGTCTTCTGCTTG
TruSeq Indexed Adapter AD018	GATCGGAAGAGCACACGTCTGAACTCCAGTCACGTCCGCATCTCGTATGCCGTCTTCTGCTTG
TruSeq Indexed Adapter AD019	GATCGGAAGAGCACACGTCTGAACTCCAGTCACGTGAAAATCTCGTATGCCGTCTTCTGCTTG

Table S4 Illumina sequencing results

	Transposition library	Lethal insertions	Lethal insertion subsets	
			Subset 1	Subset 2
Number of sequencing runs	3	1	1	1
Number of 36-bp reads mapped to Chromosome IX	14,000,357	13,710,514	10,075,540	13,424,377
Number of Chromosome IX reads containing <i>NotI</i>	96,569	166,135	290,126	319,434
Number of Chromosome IX reads with <i>NotI</i> in <i>NDC80</i> + promoter/terminator	93,826	N/A	N/A	N/A
Number of Chromosome IX reads with <i>NotI</i> in <i>NDC80</i>	70,215	165,414	289,470	318,637
Number of unique <i>NotI</i> sites in <i>NDC80</i>	1,074	336	320	351
Coverage of <i>NDC80</i> gene (%)	52	16	15	17
Number of unique codons containing insertions	444	162	149	165
Coverage of Ndc80 protein (%)	64	23	22	24

N/A, not applicable

Literature Cited

- GREENLAND, K. B., H. DING, M. COSTANZO, C. BOONE and T. N. DAVIS, 2010 Identification of *Saccharomyces cerevisiae* spindle pole body remodeling factors. *PLoS One* **5**: e15426.
- McDONNELL, A. V., T. JIANG, A. E. KEATING and B. BERGER, 2006 Paircoil2: improved prediction of coiled coils from sequence. *Bioinformatics* **22**: 356-358.
- MIRANDA, J. J., P. DE WULF, P. K. SORGER and S. C. HARRISON, 2005 The yeast DASH complex forms closed rings on microtubules. *Nat Struct Mol Biol* **12**: 138-143.
- POWERS, A. F., A. D. FRANCK, D. R. GESTAUT, J. COOPER, B. GRACYZK *et al.*, 2009 The Ndc80 kinetochore complex forms load-bearing attachments to dynamic microtubule tips via biased diffusion. *Cell* **136**: 865-875.
- SIKORSKI, R. S., and P. HIETER, 1989 A system of shuttle vectors and yeast host strains designed for efficient manipulation of DNA in *Saccharomyces cerevisiae*. *Genetics* **122**: 19-27.
- WEI, R. R., P. K. SORGER and S. C. HARRISON, 2005 Molecular organization of the Ndc80 complex, an essential kinetochore component. *Proc Natl Acad Sci U S A* **102**: 5363-5367.